

Image Generation Algorithms for FMCW-SAR at X-Band

S.Navneet¹, Ashish Roy², and C.Bhattacharya¹

¹Electronics Engineering Dept, DIAT, Pune - 411025, India

²Department of Electronic Science, University of Pune, Pune – 411007, India

nave1990@gmail.com

Abstract:

Synthetic aperture radar (SAR) based on frequency modulated continuous wave (FM-CW) transmission is a viable option for producing high resolution microwave imagery at low heights. In this paper, we show detailed analytical simulation for stripmap mode of FM-CW SAR imaging alongwith SAR images generated from actual airborne FM-CW radar video data collection.

Key words—FM-CW, SAR, Range-Doppler, UAV

I. INTRODUCTION

Airborne ground mapping is a fast expanding field of imaging sensors witnessing need for compact, cheap, high-resolution imaging instrumentation such as IR sensor, radar, LIDAR, etc. [1]-[4]. Small-scale civilian programs as well as large military coastline monitoring and reconnaissance missions with UAVs are driving the demand for such sensors.

Imaging at remote ranges using UAVs and similar such small platforms puts heavy constraint on power utilisation and payload weight. To be of interest to the civilian market, cost is a major factor. Radars have the capability of providing all weather and day-night operation. Image resolution in conventional radar systems is dependent on the size of the illuminated patch [5]. These limitations are overcome using synthetic aperture radar (SAR) technology. The azimuth resolution in SAR is unique to its case as it is dependent only on the along track real aperture antenna dimension. Pulsed SAR have been successfully deployed in satellite based remote sensing as well as for airborne missions. However, the power requirement and synchronisation efforts to put up a pulsed SAR instrumentation is complex while the cost and cubage are factors deterrent for small-scale airborne applications such as imaging at low heights with mini UAVs.

In recent years, there has been a growing interest in frequency modulated continuous wave (FM-CW) SAR technology for various military and civilian applications. Compared with pulsed SAR, the combination of FM-CW technology and SAR processing techniques have the advantages of small cubage, light weight, cost-effectiveness, and high resolution in the SAR image [6]. These characteristics make FM-CW SAR suitable to be deployed as payload on small unmanned aerial vehicles (UAV) for military (reconnaissance and surveillance operations) as well as for civilian applications.

In this work, a strip-map mode of operation of the FM-CW synthetic aperture radar (SAR) has been considered.

We present the analytical development of the FM-CW SAR signals at X-band. We produce both the simulation and actual SAR image generation from raw, video data for a FM-CW SAR sensor at C-band.

II. PRINCIPLE OF FM-CW SAR IMAGING

To appreciate how SAR images are generated and what ground truth they depict it is important to first understand the imaging geometry illustrated in Fig. 1. The radar is configured for strip-map mode imaging with the antenna mounted to side-look the scene of interest. In the case of FM-CW SAR, the signal bandwidth B is continuously swept over a time interval of T seconds repetitively. For the platform moving at a constant velocity v m/s, a number of sweeps are transmitted for the period of illumination over a point target. Unlike in pulsed SAR continuous reception takes place for the FM-CW instrument.

Since transmission as well as reception is continuous, mixing hardware is less complex at the SAR receiver. For the case of FM-CW transmission, the difference frequency between the transmitted chirp and delayed version of itself is a single frequency (beat signal). The frequency of this beat directly corresponds to the slant-range of the target. Thus, the de-chirped signal in frequency domain represents the range-compressed SAR image.

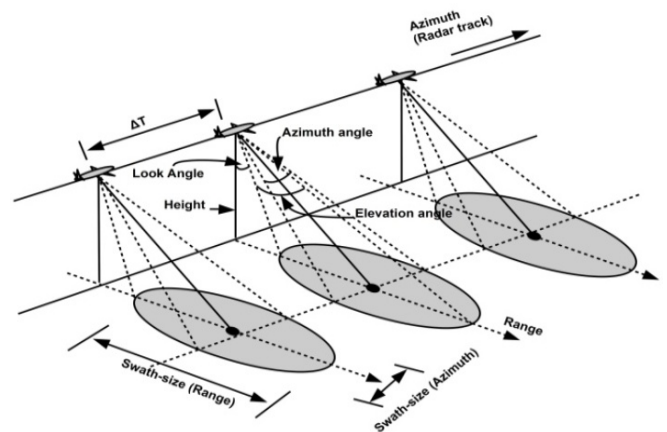


Fig. 1. FM-CW SAR geometry for stripmap imaging.

The two-way travel time τ_o to a stationary target at a cross track distance of R_o is $\tau_o = \frac{2R_o}{c}$ with the range resolution (cross track) being $\Delta r = \frac{c}{2B}$.

The transmitted waveform for the case of FM-CW SAR is

$$x(t, n) = \text{rect}\left(\frac{t}{T}\right) e^{2\pi j(f_c t + \frac{1}{2}\alpha t^2)} \quad (1)$$

The FM signal is swept at a rate of α , f_c is the carrier frequency and n denotes the sweep number while the platform is in motion with a constant velocity v .

The received signal response from a stationary point target for the n^{th} sweep interval is a time delayed version of the transmitted continuous sweep.

$$r(t - \tau_n, n) = \text{rect}\left(\frac{t - \tau_n}{T}\right) e^{2\pi j(f_c(t - \tau_n) + \frac{1}{2}\alpha(t - \tau_n)^2)} \quad (2)$$

The beat frequency ($f_n = \alpha\tau_n$) corresponds to a delay in reception for the n^{th} sweep from a point target and the two-way time delay is $\tau_n = \frac{2R_n}{c} = \frac{2\sqrt{R_o^2 + (vnT)^2}}{c}$ for the range R_n . The instantaneous beat frequency variation for a stationary point target within one sweep interval due to motion of the platform is within a single frequency bin of beat frequency measurement. Compared to the beat frequency change in consecutive sweeps because of change in R_n due to motion of the platform the instantaneous change in beat frequency from the target does not affect resolution of measurement. However, this approximation holds only for low height of imaging. The sampled beat signal at the SAR receiver is

$$s_b(i, n) = \text{rect}\left(\frac{iT_s - \tau_n}{QT_s}\right) e^{2\pi j(f_c\tau_n + i\alpha\tau_n T_s - \frac{1}{2}\alpha\tau_n^2)} \quad (3)$$

$T_s = \frac{1}{f_s}$ where f_s is the sampling rate, $0 \leq i \leq Q$, Q is the total number of samples per sweep interval containing radar returns from all the range bins in the ground swath shown in Fig. 1.

Performing a discrete Fourier transform (DFT) over (3) we have

$$S_b(k, n) = e^{\pi j(2f_c\tau_n + \alpha\tau_n T_s Q - k + \frac{k\tau_n}{T_s Q} - \alpha\tau_n^2)} \cdot \frac{\sin[\pi(\alpha\tau_n T_s - \frac{k}{Q})(Q - \frac{\tau_n}{T_s})]}{\sin[\pi(\alpha\tau_n T_s - \frac{k}{Q})]} \quad (4)$$

The beat frequency is given by DFT bin number $k = \alpha\tau_n T_s Q$. Thus, the azimuth profile of range compressed target is

$$S_b(k, n) = \exp\left(2\pi j\left(\frac{\phi_{const}}{c} f_c R_o + \frac{f_c}{cR_o} (vnT)^2\right)\right) \quad (5)$$

It can be seen from the above equation that the phase of the range compressed target is varying with the square of the sweep index n . Simulation of phase trajectory along the azimuth direction for a point target is shown in Fig. 2. Range compression causes the targets energy to lie within a single beat-frequency or range bin.

In this three-dimensional plot the ground plane represents the range-azimuth plane for a point target scatterer on ground. The z-axis represents the magnitude of

the samples of FM-signal shown in (5) for 1500 FM-CW sweeps. Therefore, the coherent integration time is $1500T$ sec, with $T = 2\text{msec}$. The FM rate of signal variation in azimuth is $K = \frac{f_c}{cR_o} (vT)^2$.

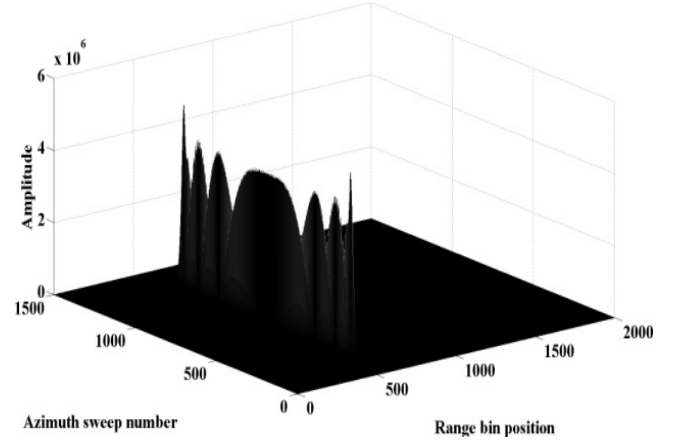


Fig. 2. Azimuth phase profile of a range compressed point target with 1500 FMCW sweeps.

Simulation of five stationary point targets is performed at X-Band. In Fig. 3, the profile of the target energy in the second curve from left is more prominent. This is because two targets are assumed to be in the same range bin at different along track locations so that the azimuth trajectory of two targets' response gets superimposed. At far ranges when the platform is at its maximum distance from the targets, a shift in bin position is observed from the curvature. Range cell migration correction similar to the case of pulsed SAR is also in order for the case of FM-CW SAR imaging. We perform azimuth compression in the Doppler (frequency) domain for the range compressed data as input.

Assume target is at along track position n_x .

$$S_b(n) = e^{2\pi j(+K(n-n_x)^2)} \quad (6)$$

A matched filter is constructed with the reference position n_r .

$$S_{match}(n) = e^{2\pi j(K(n-n_r)^2)} \quad (7)$$

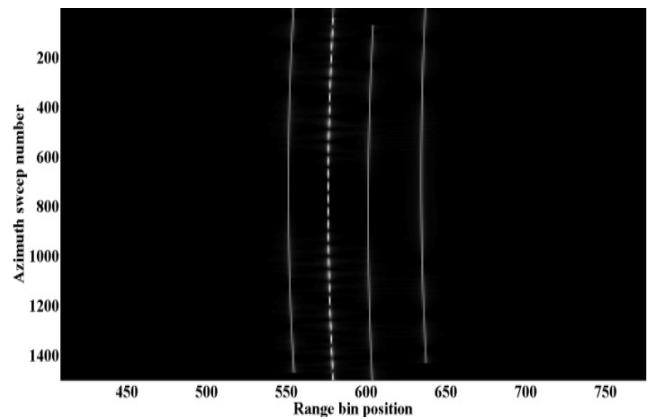


Fig. 3. 5 stationary point targets after range compression. 2 targets are at same range.

Performing the matched filter operation in azimuth in the Doppler domain as

$$F^{-1}[F[S_b(n)] * F[S_{match}^*(n)]]$$

$$L_{az}(u) = e^{\pi j(K(n_x - n_r)[N-1] + u[\frac{1}{N}-1])} \frac{\sin(\pi N(K(n_x - n_r) + \frac{u}{N}))}{\sin(\pi(K(n_x - n_r) + \frac{u}{N}))} \quad (8)$$

$$u = KN(n_r - n_x)$$

A linear relationship exists between the azimuth IDFT bin position at which the peak occurs and the azimuth spatial position of the point target coordinate on ground. The impulse response function result after matched filtering for a simulated point target is seen in Fig 4. The position of the point target as seen from the 2-D impulse response is the location of the amplitude peak on the x - y plane in the SAR image after 2-D signal compression.

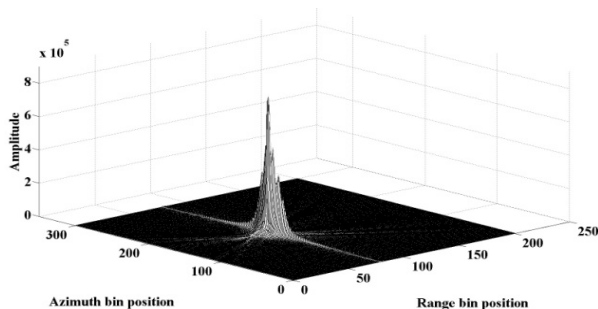


Fig. 4. 2-D impulse response function of a compressed point target.

The value of k from (4) and u from (8) give the x and y axis positions of a compressed point target peak respectively. Matched filtering operation for azimuth compression is performed on the range compressed data for the five point targets shown in Fig 3. The result of two-dimensional point target response after range-Doppler processing is as shown in Fig 5. Matched filtering in azimuth is able to extract the along track locations of the five targets from their phase histories as shown in Fig. 2. Two targets' phase trajectory which were initially superimposed on a single line as in Fig. 3 are now clearly visible post Doppler processing at their respective along track locations.

The simulation shown in Fig. 6 was performed at X-Band with an antenna length of $20cm$, platform velocity ($v=25m/s$), sweep time ($T=2ms$). The $3-dB$ width is indicated by markers on the waveform.

The azimuth axis denotes the sweep number at which the target response is maximum, giving the azimuth position of the target in the imaging scene.

Thus, impulse response width can be calculated as

$$\Delta az = v * ((2041 - 2039) * T) = 10cm,$$

which is the synthetic aperture azimuth resolution proportional to half the real aperture dimension.

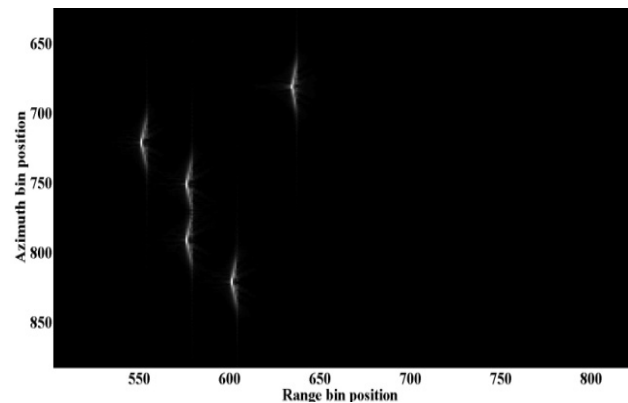


Fig 5 Compressed image of 5 point targets randomly spread on the imaging scene.

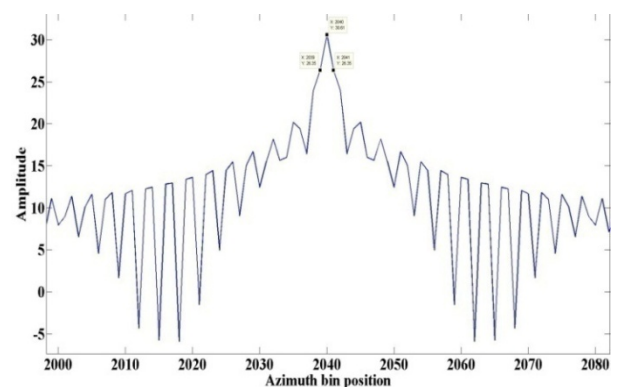


Fig 6 The azimuth impulse response function showing the azimuth resolution.

III. SIMULATION RESULTS

A sample data set (microASAR [7] data courtesy of David G. Long at Brigham Young University [8]), has been used to generate images to validate the algorithm discussed in the above section.

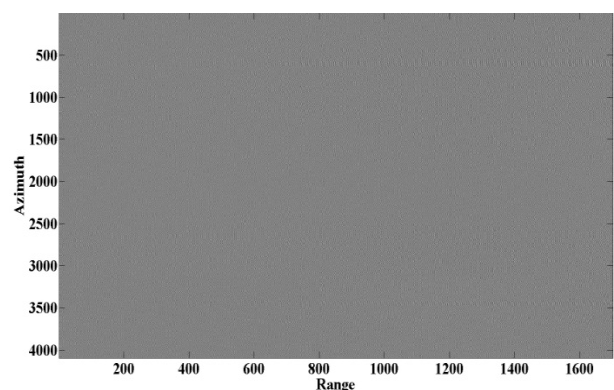


Fig 7 Raw sample backscatter data.

The raw data in Fig 7 is from a C-band FM-CW SAR payload flown on an unmanned aircraft system (UAS) as part of the Characterization of Arctic Sea Ice Experiment 2009 (CASIE-09) [9] over the Arctic Ocean from Svalbard Island. The platform manoeuvres' at an average velocity of

30.1938 m/s at an average height of 346.5029 m. The effective PRF is 307.292.

It is this data over which the range-Doppler processing is performed to generate images shown in Fig 8 and Fig 9. Multi-looking is performed to remove speckle. Underlying ground features otherwise hidden by speckle noise are prominently visible after multi-looking. Thus the analysis presented in section II is validated by real images.

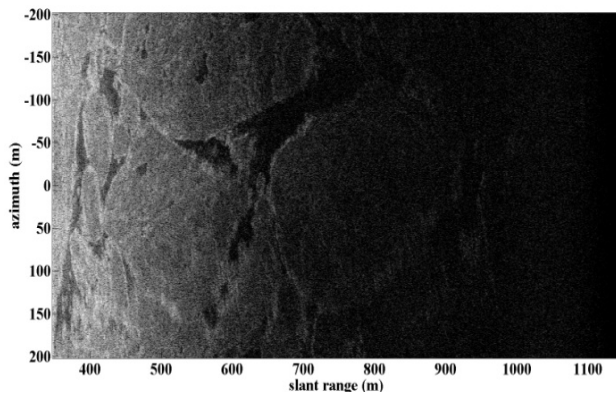


Fig 8 Single look compressed FM-CW SAR image.

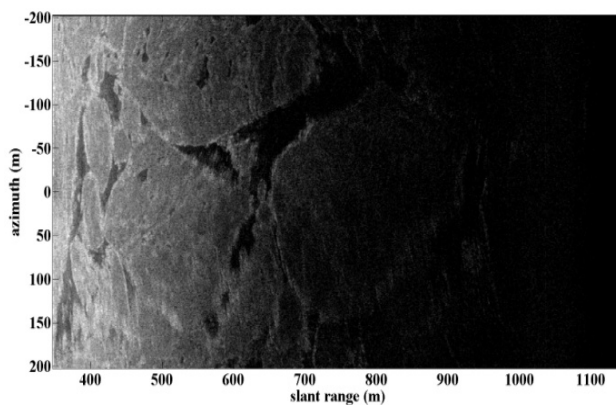


Fig 9 Multi-look compressed FM-CW SAR image (8-look).

CONCLUSION

High resolution radar imaging by FM-CW SAR instrument is worth of experimentation for producing imagery at low height and using very low power. We have produced a detailed analytical model for FM-CW radar based imaging with range-Doppler algorithm implementation. Actual SAR image clips are produced using the algorithm description in the paper.

ACKNOWLEDGEMENT

We acknowledge the project grant and support received from Vice Chancellor, DIAT, Pune and Director, SAMEER, Mumbai to conduct research and experiments for FM-CW SAR image generation.

REFERENCES

- [1] T.L. Webster, D.L. Forbes, S. Dickie and R. Shreenan, "Using topographic lidar to map flood risk from storm-surge events for Charlottetown, Prince Edward Island, Canada," *Can. J. Remote Sensing*, vol. 30, N^o 1, pp. 64-76, 2004. Paul W.Kruse, "Uncooled

Thermal Imaging", United States of America, SPIE Press.J.G.F. Francis, The QR Transformation I, 2005

- [2] Scott Hunter, Gregory Maurer, Gregory Simelgor, Shankar Radhakrishnan, John Gray, "High Sensitivity 25 μm and 50 μm Uncooled Microcantilever Infrared Imaging Arrays", SPIE Conference Proceedings, Infrared Technology and Applications, Vol 6542, 2007.
- [3] M. Rodriguez-Cassola, S. V. Baumgartner, G. Krieger, and A. Moreira, "Bistatic TerraSAR-X/F-SAR spaceborne-airborne experiment: Description, data processing and results," *IEEE Trans. Geosci. Remote Sens.*, vol. 48, no. 2, pp. 781-794, Feb. 2010.
- [4] M. I. Skolnik, "Introduction to radar systems", McGraw-Hill, Inc., London, 1980.
- [5] J. J. M. de Wit, A. Meta, P. Hoogetboom, "Modified Range-Doppler Processing for FM-CW Synthetic Aperture Radar", *IEEE Geoscience and Remote Sensing Letters* Vol. 3 No. 1, 2006, pp. 83-87.
- [6] M. Edwards, D. Madsen, C. Stringham, A. Margulis, B. Wicks, and D. Long, "microASAR: A small, robust LFM-CW SAR for operation on UAVs and small aircraft", *IEEE International Geoscience and Remote Sensing Symposium*, 2008, vol. 5, July 2008.
- [7] C. Stringham and D. G. Long, "Improved processing of the CASIE SAR data", *IEEE International Geoscience and Remote Sensing Symposium (IGARSS)*, 2011, July 2011.
- [9] J. Maslanik, R. Crocker, K. Wegrzyn, C. Fowler, U. Herzfeld, D. Long, R. Kwok, M. Fladland, and P. Bui, "Characterization of Fram Strait sea ice conditions using the NASA SIERRA unmanned aircraft system," *AGU Fall Meeting Abstracts*, vol. 1, 2009, p. 06.

BIO DATA OF AUTHOR(S)

S. Navneet was born in Chennai, India, in 1990. He received his Bachelors degree in electronics and telecommunication engineering from University of Pune, India, in 2012. He is currently working as a junior research fellow in Defence Institute Of Advanced Technology (DIAT), Pune. His research interests include signal processing, computer networks and artificial intelligence.



Ashish kr. Roy was born in West Bengal, India, in 1985. He received the MSc degree in Electronic Science in 2010 from Department of Electronic Science, University of Pune. Currently he is pursuing Ph.D from University of Pune in the field of airborne SAR signal processing. His research interests are signal processing for SAR, image processing and SAR instrumentation.



C. Bhattacharya (M'01, SM '10) received Ph.D. degree in December 2004 for his work on analysis of SAR signal correlation in scale-space framework from Jadavpur University, Kolkata. He is heading from May 2009 Electronics Engineering Department at the Defence Institute of Advanced Technology (DIAT), Pune, India, Ministry of Defence, Government of India. His research areas include signal processing for various radar and sensor configurations, stochastic processes, and bioinformatics.

